Improving coaxial measurements in laser welding by correcting distortions of a laser focus lens with a wide field of view

Jorg Entzinger,[a] Dimitrios Iakovou,[b] Ronald Aarts,[c] and Johan Meijer[d]
Mechanical Automation Laboratory, University of Twente, Faculty of Engineering Technology Horst-CTW, P.O. Box 217, 7500 AE Enschede, The Netherlands

(Received 15 June 2006; accepted for publication 22 September 2006; published 12 June 2007)

A compact, lightweight, and multifunctional head for robotic laser welding applications has been equipped with a camera to provide a real time image stream of the work piece for seam teaching, tracking, and inspection purposes [D. Iakovou, R. G. K. M. Aarts, and J. Meijer, "Integrated sensors for robotic laser welding," in *Proceedings of the Third International WLT Conference on Lasers in Manufacturing, Munich, Germany* (AT-Fachverlag GmBH, Stuttgart, 2005), pp. 121–126; D. Iakovou, R. G. K. M. Aarts, and J. Meijer "Sensor integration for robotic laser welding processes," (paper No. 2301), in Proceedings of the International Congress on Applications of Lasers and Electro-Optics (ICALEO), Miami, 2005 (unpublished)]. The camera uses part of the laser focusing optics. Research has been done to identify and correct for positioning errors introduced by the optical system. A robust camera and lens calibration method has been developed. Calibration and seam detection experiments have been performed and the results were used for seam tracking. © *2007 Laser Institute of America.*

Key words: laser welding, camera calibration, image processing, image undistortion, seam tracking

I. INTRODUCTION

Robotic laser welding is applied in many industrial environments because of the freedom to weld three-dimensional objects at high speeds. An advanced sensory system is needed to guide the welding head along the weld joint. Such a sensory system should be both compact and lightweight for reasons of accessibility and accuracy. Whereas the traditional setup consists of separate units for seam detection and tracking, laser welding, process control, and seam inspection, an integrated welding head (Fig. 1) is developed to efficiently integrate all functionality.

An image of the work piece is projected onto the camera sensor via the laser focusing lens, a dichroic mirror, and the camera lens. The laser focusing lens is optimized to focus a parallel laser beam onto a small spot on the optical axis. These type of lenses are not optimized for imaging and they are unsuitable for applications that require a large field of view. When used for imaging, a number of distortions (radial, abberations, astigmatism, etc.) will be present in the camera image. For such applications, it is of utmost importance to know the exact relation between image pixels and the real world. Therefore, the optical system has to be calibrated and distortions in the image must be corrected. The method proposed by Zhang[1] has been extended and implemented for the current research.

In the beginning of this paper (Sec. II) a concise analysis of the mathematical model of the optical system is presented. The mathematical description of the model provides extra insight for its implementation, but is not required to understand the practical use of the model which is presented in the rest of the paper.

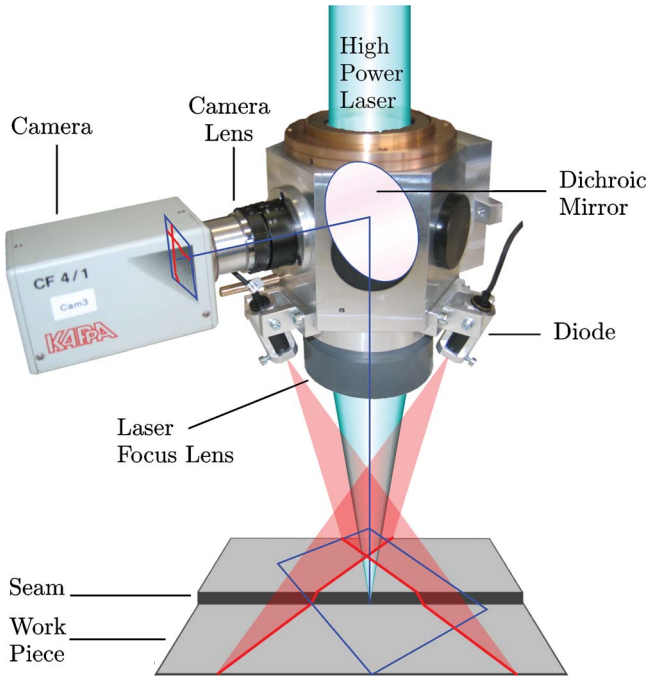

FIG. 1. Mock-up of the integrated laser welding head prototype.

[a]Electronic mail: J.O.Entzinger@alumnus.utwente.nl
[b]Electronic mail: D.Iakovou@ctw.utwente.nl
[c]Electronic mail: R.G.K.M.Aarts@utwente.nl
[d]Electronic mail: J.Meijer@ctw.utwente.nl

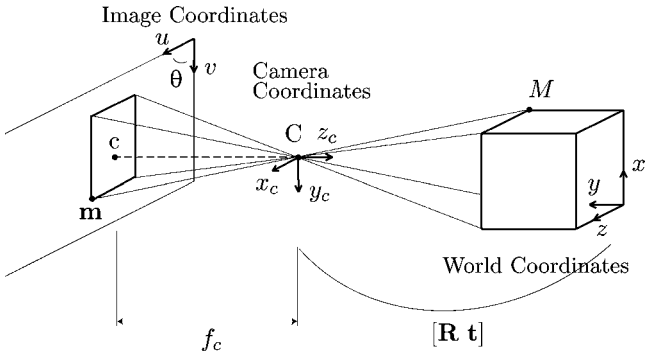

FIG. 2. Coordinate systems in projective geometry.

II. MODEL OF THE OPTICAL SYSTEM

"Distortion" is defined as *a lack of proportionality in an image resulting from defects in the optical system.*[2] This rules out the viewpoint-dependent transformations, because they do not originate from the optical system. It also rules out lens effects like spherical aberrations and astigmatism, because they do not introduce a lack of proportionality in the image, but only a blurring effect.

The imaging part of the optical system consists of the camera, the camera lens, and the laser focus lens. As a simplification, the camera lens and laser focus lens are treated as a single lens.

Figure 2 shows a transformation according to a pinhole camera model[3] where all light rays traveling through the pinhole construct an image at the virtual image plane.

A. Camera Model

The camera position and orientation $[x_c, y_c, z_c]$ are expressed relative to the world coordinates $[x, y, z]$ using a rotation and translation transformation $[\mathbf{R}\ \mathbf{t}]$. The focal length f_c of the optical system is the distance from the pinhole to the image plane. The principal point $c=[u_0, v_0]$ is the point where the optical axis crosses the image plane. The principal point is defined in the image coordinates u and v with the unit "pixels." The axes u and v are not necessarily perpendicular, nor equally scaled.

In this paper the tilde, like in $\tilde{\mathbf{v}}$, will be used to denote an augmented vector $[\mathbf{v}^T 1]^T$.

A point M in real world coordinates can be expressed in camera coordinates (M_c) using the rotation matrix $\mathbf{R}$ and translation $\mathbf{t}$ as follows:

$$M_c = \mathbf{R}M + \mathbf{t},$$

$$= \underbrace{\begin{bmatrix} r_{11} & r_{12} & r_{13} & \Delta x \\ r_{21} & r_{22} & r_{23} & \Delta y \\ r_{31} & r_{32} & r_{33} & \Delta z \end{bmatrix}}_{\mathbf{R}\quad\quad\quad\quad\quad\quad\quad\quad\mathbf{t}} \begin{bmatrix} x \\ y \\ z \\ 1 \end{bmatrix},$$

$$= [\mathbf{R}\ \mathbf{t}]\tilde{M}. \tag{1}$$

for a flat calibration object, the world coordinate z can be chosen 0 (i.e., the pattern is considered to exist in the xy plane). Therefore, without loss of generality, we can use

$$M_c = [\mathbf{R}\ \mathbf{t}]\tilde{M} = \begin{bmatrix} r_{11} & r_{12} & \Delta x \\ r_{21} & r_{22} & \Delta y \\ r_{31} & r_{32} & \Delta z \end{bmatrix} \begin{bmatrix} x \\ y \\ 1 \end{bmatrix}. \tag{2}$$

The parameters $\mathbf{R}$ and $\mathbf{t}$ are the camera *extrinsic parameters*, as they specify a transformation outside the camera system.

The 3D point M is projected onto the 2D image plane resulting in point $\mathbf{m}=[u, v]$ by the projection

$$\frac{u}{x_c} = \frac{v}{y_c} = \frac{f_c}{z_c}, \tag{3}$$

or, in matrix-vector form (with s set equal to z_c by the lower row in the equation),

$$s\begin{bmatrix} u \\ v \\ 1 \end{bmatrix} = \begin{bmatrix} f_c & 0 & 0 \\ 0 & f_c & 0 \\ 0 & 0 & 1 \end{bmatrix} \begin{bmatrix} x \\ y \\ z \end{bmatrix}_c. \tag{4}$$

Including the camera parameters θ, u_0, and v_0 in this transformation gives the full camera transformation:

$$s\begin{bmatrix} u \\ v \\ 1 \end{bmatrix} = \begin{bmatrix} f_c k_u & f_c k_u/\tan\theta & u_0 \\ 0 & f_c k_v/\sin\theta & v_0 \\ 0 & 0 & 1 \end{bmatrix} \begin{bmatrix} x \\ y \\ z \end{bmatrix}_c. \tag{5}$$

The variables k_u and k_v in this equation specify the real world pixel sizes in the u and v direction, respectively. The parameters in this transformation specify the internal behavior of the camera. These parameters are the camera *intrinsic parameters*.

A change in the focal length f_c in Eq. (5) cannot be distinguished from a change in the pixel dimensions k_u and k_v. The magnifying part f has been split off for reasons of convenience. The zooming part of the camera intrinsic matrix, which is the upper-left 2×2 matrix, is normalized to be nonmagnifying:

$$s\begin{bmatrix} u \\ v \\ 1 \end{bmatrix} = \underbrace{\begin{bmatrix} \alpha & \gamma & u_0 \\ 0 & \beta & v_0 \\ 0 & 0 & 1 \end{bmatrix}}_{\mathbf{A}} \underbrace{\begin{bmatrix} f & 0 & 0 \\ 0 & f & 0 \\ 0 & 0 & 1 \end{bmatrix}}_{\mathbf{F}} \begin{bmatrix} x \\ y \\ z \end{bmatrix}_c,$$

or

$$s\tilde{\mathbf{m}} = \mathbf{A}\mathbf{F}M_c, \tag{6}$$

with

$$\left\| \begin{matrix} \alpha & \gamma \\ 0 & \beta \end{matrix} \right\|_{\mathrm{Fro}} = \sqrt{2}, \tag{7}$$

and thus

$$f = \frac{\left\| \begin{matrix} f_c k_u & f_c k_u/\tan\theta \\ 0 & f_c k_v/\sin\theta \end{matrix} \right\|_{\mathrm{Fro}}}{\sqrt{2}}, \tag{8}$$

where Fro is the Frobenius norm.

A point expressed in the camera coordinate system can now be projected onto the image plane by Eq. (6). Using the

combination of Eq. (1) and Eq. (6) a translation from real world coordinates—or an ideal model—to image coordinates can be made.

B. Lens Model

Besides the camera imperfections modeled by the intrinsic parameters, there are distortions introduced by the lenses. Most lens distortions are dominated by radial distortions and especially by the first order radial distortion. In literature often the first two radial distortions[1,4,5] and sometimes also two tangential distortion components are taken into account.[6] It is most important to correct for these distortions and therefore to accurately estimate the distortion parameters.

In the following formulas, a breve ($\breve{}$) denotes a distorted coordinate, with subscripts r and t to indicate radial and/or tangential distortion. For readability the subscript c for camera coordinates is left out.

The transformation from the ideal points x and y to the radially distorted points $\breve{x}_r$ and $\breve{y}_r$ is described by

$$\breve{x}_r = x + x[\kappa_1(x^2+y^2) + \kappa_2(x^2+y^2)^2], \tag{9}$$

$$\breve{y}_r = y + y[\kappa_1(x^2+y^2) + \kappa_2(x^2+y^2)^2], \tag{10}$$

where κ_1 and κ_2 are the first and second order radial distortion parameters. The addition of two tangential distortion parameters τ_1 and τ_2 is given by

$$\breve{x}_{rt} = \breve{x}_r + \tau_1(3x^2+y^2) + 2\tau_2 xy, \tag{11}$$

$$\breve{y}_{rt} = \breve{y}_r + 2\tau_1 xy + \tau_2(x^2+3y^2). \tag{12}$$

The fact that the lens is fixed to the camera means that lens distortions should be added to the model after the real world to camera coordinates transformation (but before the perspective projection). The zooming matrix **F** can be put on either side of the lens distortion transformation, as it is just a linear scaling. Here it was chosen to keep **F** with the [**Rt**] matrix. To find the radially distorted image coordinates $\breve{u}$ and $\breve{v}$ in terms of the ideal coordinates we use

$$\breve{u} = u_0 + \alpha\breve{x} + \gamma\breve{y},$$

$$\breve{v} = v_0 + \beta\breve{y}. \tag{13}$$

Substitution of Eq. (9) and Eq. (10) gives

$$\begin{aligned}\breve{u}_r &= u_0 + \alpha x + \alpha x[\cdots] + \gamma y + \gamma y[\cdots] \\ &= \underbrace{u_0 + \alpha x + \gamma y}_{=u} + \underbrace{\alpha x[\cdots] + \gamma y[\cdots]}_{=(u-u_0)[\cdots]} \\ &= u + (u-u_0)[\kappa_1(x^2+y^2) + \kappa_2(x^2+y^2)^2]\end{aligned} \tag{14}$$

and

$$\begin{aligned}\breve{v}_r &= v_0 + \beta y + \beta y[\cdots] \\ &= \underbrace{v_0 + \beta y}_{=v} + \underbrace{\beta y[\cdots]}_{=(v-v_0)[\cdots]} \\ &= v + (v-v_0)[\kappa_1(x^2+y^2) + \kappa_2(x^2+y^2)^2].\end{aligned} \tag{15}$$

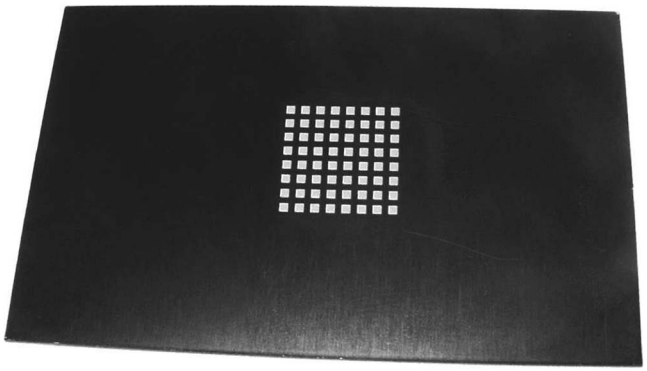

FIG. 3. Calibration pattern laser engraved in anodized aluminum. The pattern size is circa 15×15 mm.

The same substitution can be done for the tangential additions, which results in

$$\breve{u}_{rt} = \breve{u}_r + \alpha\tau_1(3x^2+y^2) + \alpha 2\tau_2 xy + \gamma 2\tau_1 xy + \gamma\tau_2(x^2 + 3y^2), \tag{16}$$

$$\breve{v}_{rt} = \breve{v}_r + \beta 2\tau_1 xy + \beta\tau_2(x^2+3y^2). \tag{17}$$

III. ACQUISITION OF CALIBRATION DATA

The calibration procedure relies on the comparison of (distorted) feature points extracted from images taken using the optical system under investigation on one side, with the ideal model feature points transformed using the camera and lens models on the other. To be able to eliminate the camera extrinsic parameters ([**Rt**]) several pictures of a calibration pattern (like the one in Fig. 3) must be taken under different orientations. As the intrinsic parameters (i.e., camera and lens transformations) will be the same for all images and the extrinsic parameters (i.e., rotation and translation) will differ, it is possible to differentiate between these parameters (see also Sec. IV).

A. Feature Point Extraction

Once images of the calibration pattern are available, the feature points must be extracted. After a compensation for nonhomogeneous lighting, all calibration objects (in this example squares) are identified. This is done using thresholding and labeling functions, followed by a selection of only those labeled objects that have a large enough area. The four object corners are identified as the pixels furthest away from the object's center of gravity, with the constraint that two corners cannot be closer to each other than a specified number of pixels.

For clear images, like Zhang's test images [Fig. 4(a)] or images taken with a photo camera, the proposed method performs sufficiently. For the images taken using the integrated welding head [Fig. 4(b)] it is more difficult to identify corners properly, as the reduced image quality makes it very sensitive to different thresholding values.

For these blurry images it is better to use the object centroids as feature points instead of the corners. Although after perspective distortion the centroid will be shifted

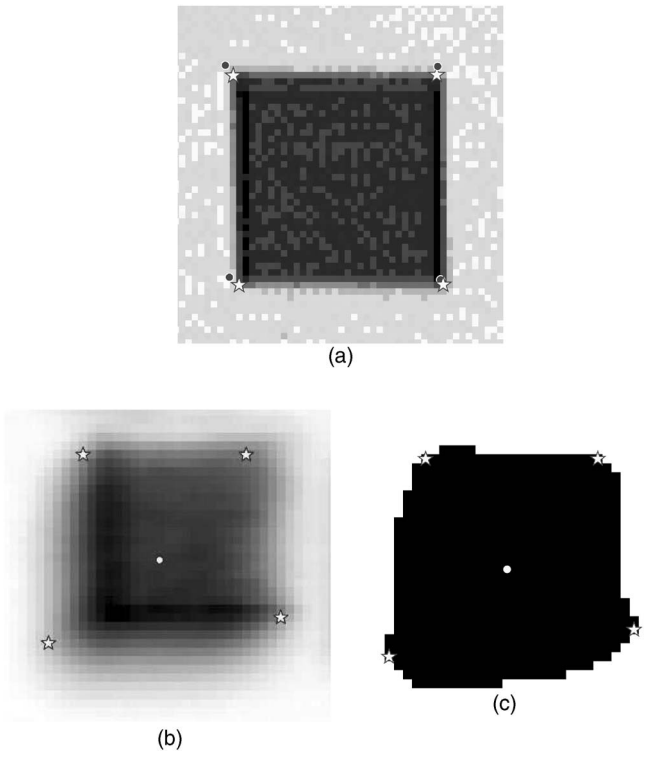

FIG. 4. Determination of corner points. (a) Cut-out of an image by Zhang; extracted feature points depicted as stars and Zhang's data (with software by Brian Guenter) depicted as dots. (b) Feature points determined for the welding head image; determining a proper threshold level is difficult, but critical. (c) Cut-out of a thresholded image (b); it is difficult to indicate where the corners are.

slightly, the accuracy of detection is high. The shift of the centroid is negligible, because the rotations of the pattern should be small to stay within the focal range.

For the images taken using the integrated welding head it was found that an intensity weighted approach gives the best results. This method uses an initial (too tight) threshold to globally identify the calibration objects. A region around the initially identified objects is then selected, in which the (normalized) intensity determines the contribution of a pixel to the object's centroid.

B. Feature Point Ordering

The extracted feature point coordinates should be listed in the same order as the coordinates in the ideal model. How they are ordered is not important, as long as the model points and the extracted points can be matched. An algorithm has been developed to automate the ordering process. An example is displayed in Fig. 5.

IV. CAMERA AND LENS PARAMETER DETERMINATION

To find the camera and lens parameters an implementation of the algorithm in Ref. 1 was used, with the adaptation of keeping a constant zooming factor in the **A** matrix as pointed out in Sec. II A.

A. Algorithm in Brief

In this algorithm first a homography

$$\mathbf{H} = \mathbf{AF}[\mathbf{R}\ \mathbf{t}] \tag{18}$$

is calculated for every image. Actually **H** is the best fit between the model points and the extracted feature points according to

$$s\tilde{\mathbf{m}} = \mathbf{H}\tilde{M} \tag{19}$$

[compare with the combination of Eq. (2) and Eq. (5)].

As s in Eq. (19) can be scaled arbitrarily, the 3×3 matrix **H** has 8 degrees of freedom. Rotation and translation can be fully described with 6 independent parameters, which means that two constraints can be formulated on **H**. These constraints can be found in the orthonormality of **R**. With the two constraints on each homography, it follows that at least 3 images are needed to solve for the 5 independent camera intrinsic parameters in **AF**.

Once initial estimates are present for **AF** and the [**Rt**] matrices, an initial estimate for the lens distortions can be calculated. The radial distortion parameters κ_1 and κ_2 can be calculated by using the pseudoinverse to solve the matrix-vector form of Eq. (14) and Eq. (15):

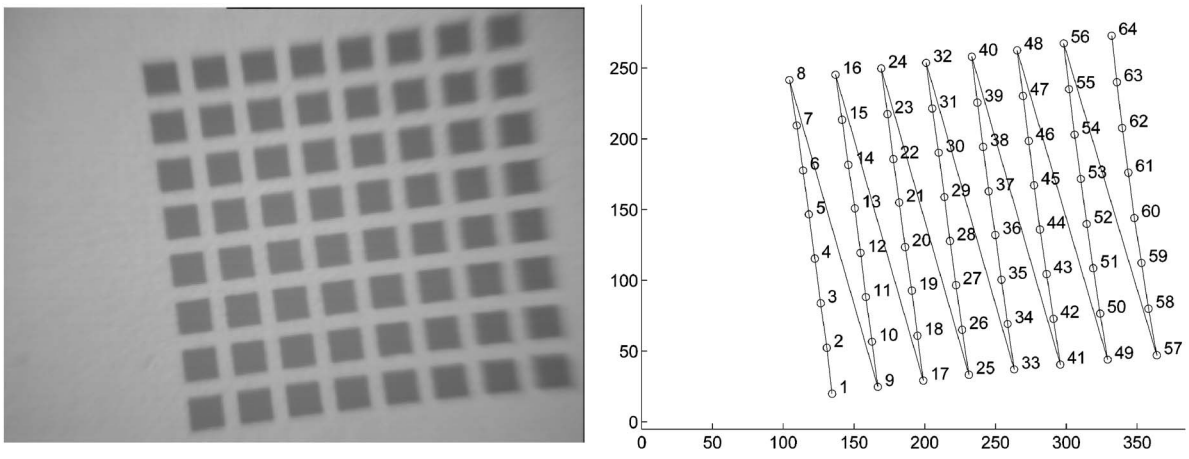

FIG. 5. The original image (left) and the extracted object centroid feature points in order (right).

$$\begin{bmatrix} (u-u_0)(x^2+y^2) & (u-u_0)(x^2+y^2)^2 \\ (v-v_0)(x^2+y^2) & (v-v_0)(x^2+y^2)^2 \end{bmatrix} \begin{bmatrix} \kappa_1 \\ \kappa_2 \end{bmatrix} = \begin{bmatrix} \breve{u}-u \\ \breve{v}-v \end{bmatrix}. \tag{20}$$

The radial plus tangential distortions from Eq. (16) and Eq. (17) can be solved in a similar way.

A nonlinear least squares parameter optimization is performed to refine all estimates. All parameters are optimized simultaneously. To reduce the number of parameters to optimize and to make sure an unconstrained optimization can be carried out, the rotation matrices are exchanged by their Rodrigues parameters.[7]

B. How to Cope With Images of Bad Quality

In case of poor quality calibration images the accurate extraction of feature point coordinates becomes more difficult. In those cases the calibration results may vary considerably depending on the calibration images used. To overcome this, a manifold (typically 2000–3000) of subsets of four images are analyzed. The results of the subsets with the best fits between the extracted feature points and the transformed model points (lowest rms values in nonlinear LSQ optimization) are generally the best to use for undistortion.

A comparative analysis of (averaged) parameter sets can be done using the original calibration images. For this analysis images are undistorted using the selected parameters and all rows and columns of feature points are fit to straight lines. All fitting residuals are summed and compared to fitting residuals obtained from the original (distorted image) feature points. Apart from noise in the data sets, this offers a good possibility to compare different parameter sets. Differences in selection criteria for subset results and in thresholding settings have been analyzed this way.

V. IMAGE UNDISTORTION

Most procedures discussed in literature use the inverse of the distortion function to undo images from their distortions. For the distortion functions Eq. (14) and Eq. (15) used in this paper an iterative process is needed. Other research has focused on developing distortion functions that can easily be inverted.[5]

All these efforts seem unnecessary if we realize that we can just distort any image according to the result of the camera-lens calibration. The calibration provides information about the displacement of the pixels in the real world into the camera image. Therefore, if we assume that an undistorted image of the real world exists in the form of an empty look-up table (LUT), then distorting this LUT with the results acquired by the calibration will produce a LUT in the way that it would be viewed by the camera [Fig. 6(a)]. Then the undistortion of an image becomes a simple step of retrieving the intensity of the distorted LUT [Fig. 6(b)].

This newly developed technique is practical, accurate, and fast, and for a real-time implementation things can be speeded up even more. A file with undistortion parameter values is read upon the program start-up and a lookup table is created defining for every point in the undistorted image, from which pixel in the distorted image the intensity should be taken. In real time, the only thing that needs to be done is to apply the lookup table to transform the image pixels, which is very fast. Interpolation could be done, but this will slow down the undistortion process.

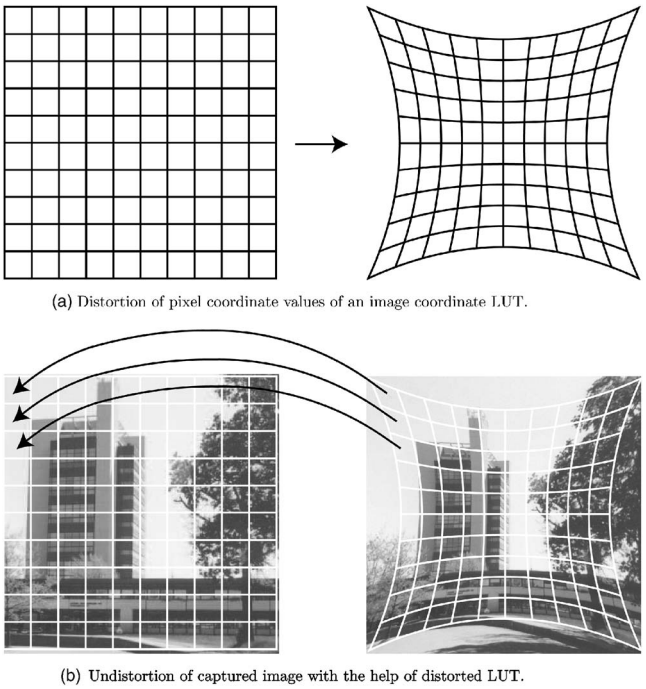

(a) Distortion of pixel coordinate values of an image coordinate LUT.

(b) Undistortion of captured image with the help of distorted LUT.

FIG. 6. Use of look-up tables to undistort images.

VI. CAMERA-LENS CALIBRATION

The calibration process involves the practical implementation of the steps that were described in the previous paragraphs. The calibration needs to be performed only once and is valid for as long as the optical path and components, viewing direction, and orientation of the camera remain unchanged.

The first step is to capture images of the pattern like the one shown in Fig. 3 with the implemented optical setup. The calibration pattern is placed at the focal distance of the high power laser focus lens with different orientations in relation to the system's optical axis. The full pattern shape must be visible inside the image frame.

The next step is to detect and order the feature points of the calibration pattern as explained in Sec. III and to determine the camera and lens parameters as explained in Sec. IV.

Zhang's calibration results have been verified with the current implementation. Both for the available data sets and for feature points extracted from Zhang's images, the estimated parameters and the undistortion results are well in line with his results in in Ref. 1.

Calibrations with simulated images and data sets and with real images have shown that small rotations of the calibration pattern ($\pm 5^\circ$) around the optical system's focal plane are beneficial for an accurate estimation of the (radial) distortions, while large rotations (20–45°) result in a more ac-

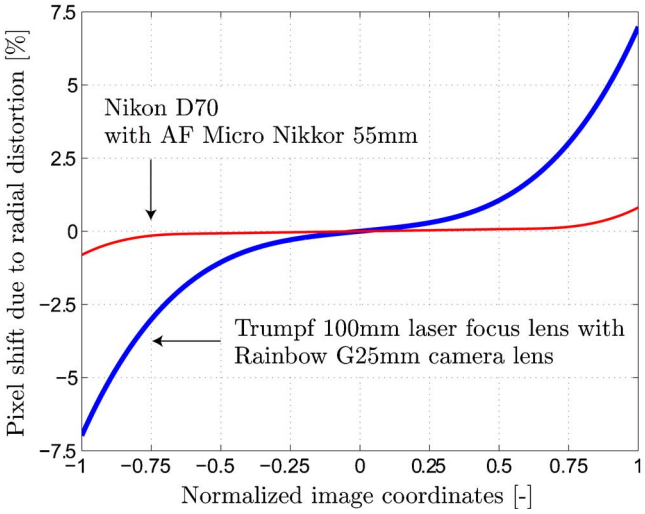

FIG. 7. Shift of pixel data due to radial distortions. The shift percentage is plotted against the distance from the image center. The thin line is for the photo camera, the thick line is for the welding head.

curate estimation of the zooming factor f. As f is not a parameter needed for the undistortion of images, small rotations of the pattern and the proposed separation of the camera parameters and f during the optimization process are recommended.

A. Calibration experiments

A semiprofessional digital photo camera has been calibrated as a test case. Because the lenses used for photo cameras are optimized for imaging, images are much clearer than those taken using the welding head. Moreover, the high resolution and large field-of-depth result in much better images and feature points are much easier to detect. As expected, because of the quality of this camera and its lens, the radial distortions are very small.

The thin line in Fig. 7 shows the radial distortion for every point on the diagonal of the photo camera image. The distortions are negligible in a large central area, whereas the corners of the image moved nearly 1% (which would only be 0.75 mm when printed as a normal photo).

When calibrating the integrated welding head optics the need for camera calibration for accurate position measurements becomes clear (thick line in Fig. 7). Being almost 7.5%, the maximum distortion would be over 5 mm when printed as a photograph.

Estimations of the tangential distortions have been implemented as well. Their influence appears to be negligible compared to the radial distortions, which is in line with literature.

Calibration results based on full resolution images (768 $\times$576) or subsampled images (384$\times$288) did not show significant results. In Fig. 8(a), radial distortions are responsible for the deformation of the structured laser lines on the captured image. After undistortion the laser lines appear straight again in Fig. 8(b).

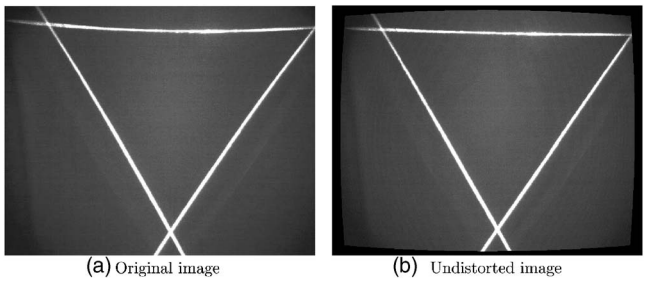

FIG. 8. Radial distortions that are present in the original image (curved lines) are corrected with undistortion.

B. Imaginary calibration results

In some tests imaginary calibration results showed up in the calculation of the camera intrinsic parameters (Sec. IV A). This is due to badly conditioned matrices, caused by highly correlated or contradicting input data. Imaginary data can also appear when one data set was used multiple times as input for a single calibration. In the current implementation, if imaginary results are detected, then calibration is terminated for the subset in question.

A remarkable improvement of the overall result can be obtained by leaving out images that often occur in sets with imaginary results. An example of such an improvement is illustrated in Fig. 9, where the rms values resulting from the nonlinear LSQ optimization (Sec. IV B) are presented. If the images that often occur in sets that provide imaginary results are allowed to participate in other image subsets, a frequency histogram like the one of Fig. 9(a) results, whereas in the case where those images are not allowed to further participate in the parameter estimation the result of Fig. 9(b) is obtained. By comparing the two figures it is obvious that the omitted images do not contribute to the occurrence of small rms values but on the contrary they mainly result in higher ones. The most important aspect is that these image sets do not only influence the rms value, but also the first radial distortion parameter κ_1 and the factor f parameters. Therefore, it is important to be able to discard bad data by reviewing the results and checking how often and when a certain image is linked to the presence of imaginary results.

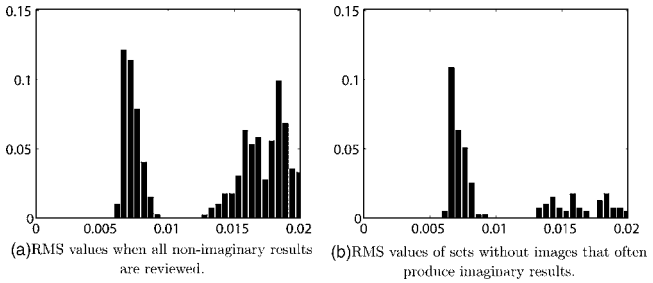

FIG. 9. The images that often occur in sets with imaginary results mainly contribute to the occurrence of high rms values.

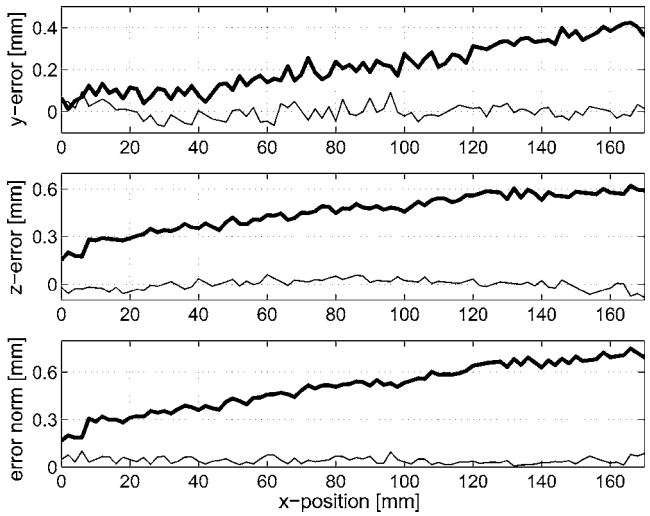

FIG. 10. Distance between the points measured from distorted images (thick line), with respect to a line fit through the undistorted measurements (thin line).

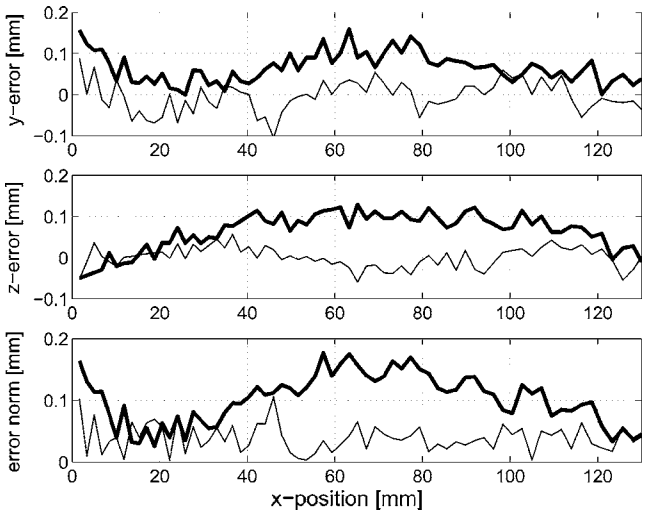

FIG. 11. Accuracies from measurements on the curved seam test object. The thick line represents the original (distorted) situation; the thin line is obtained using image undistortion.

VII. SEAM DETECTION RESULTS

Several seam detection experiments have been carried out with and without image undistortion. As could be expected, image undistortion is beneficial to the improvement of the measurement accuracy of the seam position. The results of two of those experiments are presented further in this section. In these two experiments the sensor moves along a straight line. Every two millimeters the sensor performs measurements on the seam that is placed beneath it. The further a seam point exists from the sensor path, the less accurate its position measurement is due to distortions. For the current experiments a CCD camera of 384×288 pixels was used.

The first experiment involves the detection of a straight seam. The seam is positioned in such a way under the sensor that its initial position will appear around the center of the sensor image (therefore very little or no radial distortions exist) and gradually move towards the outer parts of the image where the correction of radial distortions is necessary. As displayed in Fig. 10, there is a significant difference between the measurements of the distorted (thick line) and undistorted (thin line) images. Even though the accuracy of the measurements has been improved with undistortion, there still exist errors of almost 100 μm. This is the limit of the accuracy necessary for laser welding. Further improvements can be possible with the use of higher resolution cameras.

In the second experiment the straight seam is replaced by a curve which is part of a circle with radius 182 mm. The curved seam is placed under the sensor in such a way that it crosses the linear path of the sensor twice. This means that the beginning and the end of the curve exist on one side of the linear path of the sensor, whereas the rest of the curve on the other side. In Fig. 11 the measurement errors of the distorted (thick line) and undistorted (thin line) data are displayed. The shown errors are computed distances of the measurements with a fitted circle through the undistorted data. Similar conclusions to the ones of the linear seam can be made in this case as well. The difference between the distorted and undistorted measurement errors is smaller. This is because the furthest point on the curve does not reach the outer parts of the sensor's image plane as was the case with the straight line seam.

VIII. DEVELOPED TOOLBOX

Even though the steps of the camera and lens calibration are explicit, the process itself is quite complex and multivariable. Therefore, there is a need for a tool that allows a user to perform such a calibration without having to know all the details of the process. For this reason an automated calibration toolbox was developed with a graphic user interface that guides the inexperienced user through the calibration process, but also provides the ability for the experienced user to interact during the process. This toolbox has been developed under MATLAB.

The user can define the type of calibration pattern that is used and the type of undistortions that are required to be detected. Furthermore, the detection algorithm for the key point extraction can be selected as well as the type of key points that are to be detected (centroid, corner). Additional to the toolbox's image selection mechanism the user is also allowed to manually omit undesired images, as well as to view the process of the parameter estimation and its intermediate results.

Finally, the user can view and undistort any image according to the estimated parameters, and repeat any part of the calibration process if any further optimization is required. The process also produces a calibration file that can be used from applications outside the GUI for undistortion.

IX. CONCLUSION

The desire for a compact and multifunctional laser welding head as expressed by the industry comes with several technological challenges. One of these challenges is compensation of the radial distortions present in images for seam tracking and inspection. Due to the fact that the laser focus

lens has not been optimized for imaging purposes, a robust camera and lens calibration procedure is needed. A tool to assist the parameter estimation process of the calibration is developed, which also makes possible the visualization of the intermediate and final calibration results. This research has shown that the image undistortion can be achieved easily.

ACKNOWLEDGMENTS

This work is financially supported by the Dutch Technology Foundation STW under Grant No. TWO.5927.

[1]Z. Zhang, "A flexible new technique for camera calibration," Technical Report MSR-TR-98-71, Microsoft Research, December 1998. See http://research.microsoft.com/~zhang/Calib/.

[2]Merriam-Webster Inc., *Merriam-Webster's Collegiate Dictionary*, 2000. See http://www.m-w.com/.

[3]G. Xu and Z. Zhang, "Epipolar Geometry in Stereo, Motion and Object Recognition-A Unified Approach," *Computational Imaging and Vision*, 6th ed. (Kluwer Academic, Dordrecht, 1996).

[4]X. Jian, A. A. Malcolm, and F. Zhongping, "Camera calibration with micron level accuracy," Technical Report AT/01/037/PS, Singapore Institute of Manufacturing Technology, 2001. See http://www.simtech.a-star.edu.sg/research/TechnicalReports/TR0090.pdf.

[5]L. Ma, Y. Q. Chen, and K. L. Moore, "A new analytical radial distortion model for camera calibration," *CoRR: Computer Vision and Pattern Recognition*, 2003. See http://arxiv.org/PS_cache/cs/pdf/0307/0307046.pdf.

[6]D. C. Brown, "Close-range camera calibration," Photogramm. Eng. **37**, 855–866 (1971).

[7]E. W. Weisstein *et al.*, "Rodrigues' rotation formula," *From MathWorld-A Wolfram Web Resource*, 2005. See http://mathworld.wolfram.com/RodriguesRotationFormula.html.